NANO LETTERS

pubs.acs.org/NanoLett Letter

Unconventional Pressure-Driven Metamagnetic Transitions in Topological van der Waals Magnets

Tiema Qian,[§] Eve Emmanouilidou,[§] Chaowei Hu, Jazmine C. Green, Igor I. Mazin, and Ni Ni*

Cite This: *Nano Lett.* 2022, 22, 5523−5529 Read Online

ACCESS | Metrics & More | Article Recommendations | Supporting Information

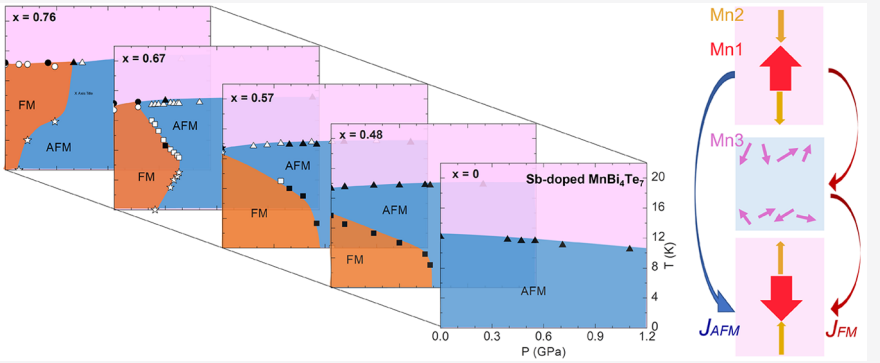

ABSTRACT: Activating metamagnetic transitions between ordered states in van der Waals magnets and devices bring great opportunities in spintronics. We show that external pressure, which enhances the interlayer hopping without introducing chemical disorders, triggers multiple metamagnetic transitions upon cooling in the topological van der Waals magnets $Mn(Bi_{1-x}Sb_x)_4Te_7$, where the antiferromagnetic interlayer superexchange coupling competes with the ferromagnetic interlayer coupling mediated by the antisite Mn spins. The temperature−pressure phase diagrams reveal that while the ordering temperature from the paramagnetic to ordered states is almost pressure-independent, the metamagnetic transitions show nontrivial pressure and temperature dependence, even re-entrance. For these highly anisotropic magnets, we attribute the former to the ordering temperature being only weakly dependent on the intralayer parameters and the latter to the parametrically different pressure and temperature dependence of the two interlayer couplings. Our independent probing of these disparate magnetic interactions paves an avenue for efficient magnetic manipulations in van der Waals magnets.

KEYWORDS: *pressure, van der Waals material, magnetic topological insulator, phase diagram*

Van der Waals (vdW) magnets have laid the material foundation for engineering two-dimensional (2D) thin-film devices and heterostructures with intrinsic magnetism. Triggering metamagnetic transitions between ordered states and understanding how such manipulations are driven open up unprecedented opportunities in magneto-electronics, spintronics, and topotronics.[1−14] Versatile means, including layer-thickness engineering, electrogating, chemical doping, strain, pressure, etc., have been actively explored to modify the three major interactions including magnetic anisotropy and interlayer and intralayer magnetic couplings, with the aim of tuning the competing magnetic states. However, due to the lack of vdW magnets with comparable ferromagnetic (FM) and antiferromagnetic (AFM) energies, despite extensive efforts, the activation of the metamagnetic transitions between these two states has only been unambiguously experimentally realized in CrI_3 and CrSBr insulators,[8−16] and there they are likely triggered by the structural changes. This has hindered progress in understanding the roles that these disparate magnetic interactions play in driving such transitions.

Recently, the $MnBi_{2n}Te_{3n+1}$ (MBT) family has been discovered to be intrinsic vdW magnets with nontrivial band topology.[17−30] They are composed of alternating $(n-1)$ $[Bi_2Te_3]$ quintuple layers (QLs) and one $[MnBi_2Te_4]$ septuple layer (SL). In the 2D limit of $MnBi_2Te_4$, due to the interplay of magnetism and band topology, emergent phenomena including the quantized Hall conductance, Chern insulator state, and large layer Hall effect have been observed.[31−34] Besides their fascinating nontrivial band topology, this is a family with great structural and magnetic tunability. With increasing n, $MnBi_2Te_4$, $MnBi_4Te_7$, and $MnBi_6Te_{10}$ become A-type antiferromagnets, while $MnBi_8Te_{13}$ becomes FM. Particularly,

Received: April 26, 2022
Revised: June 16, 2022
Published: June 22, 2022

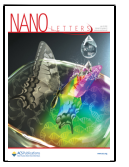

https://doi.org/10.1021/acs.nanolett.2c01680
Nano Lett. 2022, 22, 5523−5529

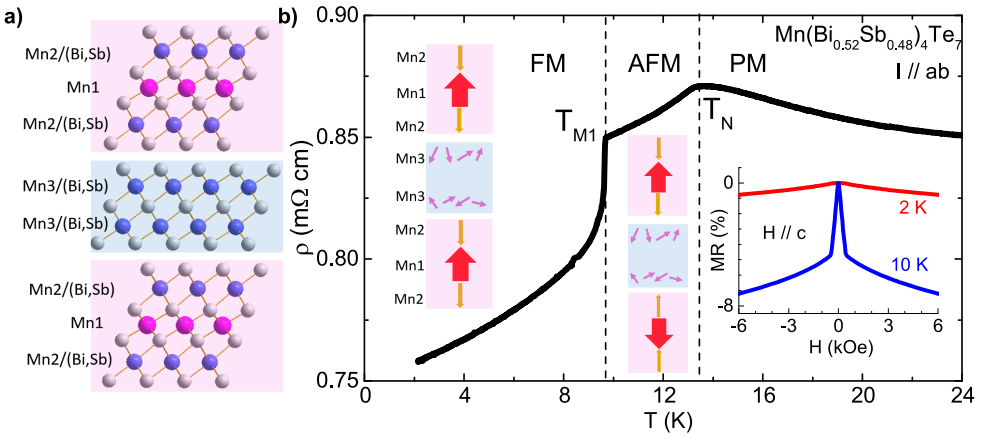

Figure 1. (a) Crystal structure of $Mn(Bi_{1-x}Sb_x)_4Te_7$. Sb doping can introduce $Mn_{(Bi, Sb)}$ antisites. Mn1 represents the Mn atoms on the Mn site; Mn2 labels the Mn atoms on the (Bi, Sb) site in the SLs; Mn3 denotes the Mn atoms on the (Bi, Sb) site in the QLs. (b) Temperature-dependent resistivity, $\rho(T)$ of $x = 0.48$ sample under ambient pressure, with schematics of the magnetic structures.[38] Upon cooling, Mn1 sublattice undergoes PM → AFM → FM transitions. In these ordered states, Mn1 and Mn2 sublattices are always AFM to each other along the c axis while Mn3 spins are paramagnetic. Right inset: its magnetoresistance MR(H) in the FM state (2 K) and AFM state (10 K).

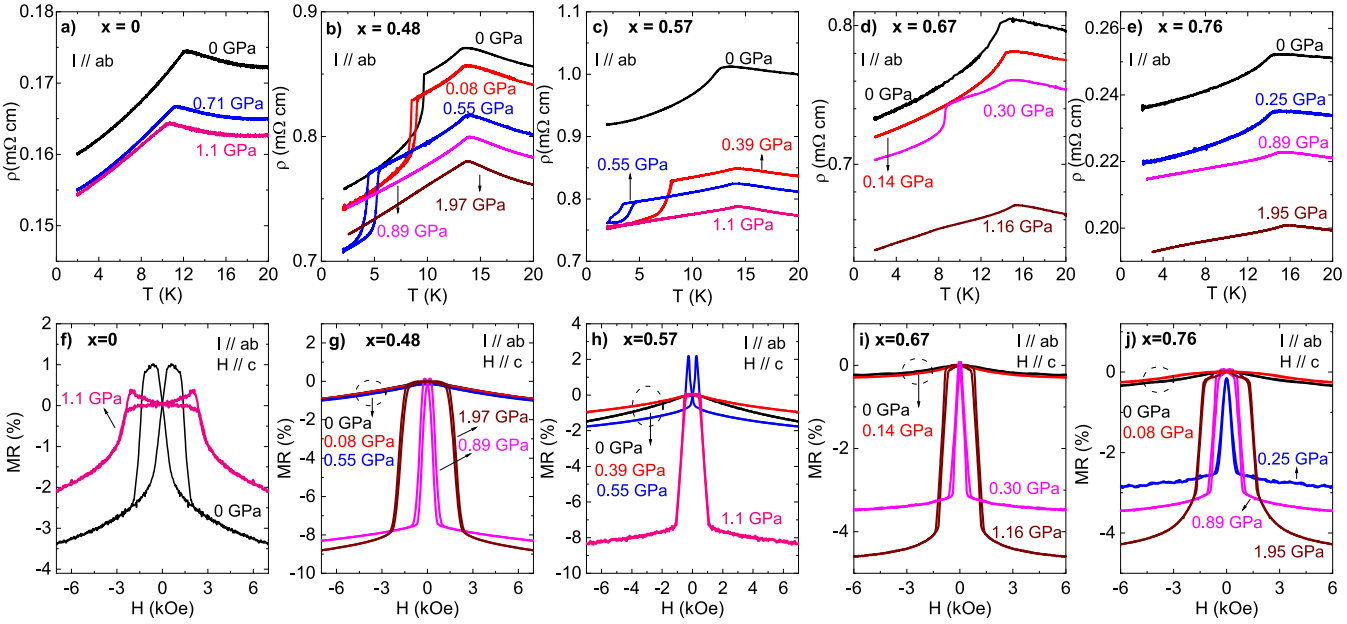

Figure 2. Effect of external pressures on the electrical properties of $Mn(Bi_{1-x}Sb_x)_4Te_7$ ($x = 0$, 0.48, 0.57, 0.67 and 0.76). (a–e) $\rho(T)$ at different pressures with the current $I//ab$ plane. (f–j) MR(H) at 2 K under pressures with $I//ab$ and $H//c$. The sharp drop in MR indicates the Mn1 spins are at the AFM state while the MR showing weak field dependence suggests FM state of the Mn1 spins.

the as-grown $MnBi_4Te_7$ and $MnBi_6Te_{10}$ may become FM under certain growth conditions,[24,35] indicating close proximity of FM and AFM energy scales in this family. Chemical doping has been used to tune the magnetism in MBT.[36−40] The effect can be best seen in $Mn(Bi_{1-x}Sb_x)_4Te_7$, where a doping-dependent metamagnetic transition between the FM and AFM states is observed.[38] However, the vacancies and antisite disorder introduced by doping are uncontrollable, making the delineation of the effects of the three major magnetic interactions challenging. Meanwhile, external pressure serves as a tuning knob without changing the chemical disorder.[41−43] However, it has been seldom applied to the MBT family where the understanding of these magnetic interactions still remain elusive.[41−44] In this Letter, using electrical transport and magnetometry measurements, we discover the extremely sensitive, nontrivial, and even re-entrant pressure-driven activation and manipulation of the metamagnetic transitions in $Mn(Bi_{1-x}Sb_x)_4Te_7$.

In $Mn(Bi_{1-x}Sb_x)_4Te_7$, Sb atoms not only replace Bi atoms but also promote site mixing between Sb and Mn. The presence of $Mn_{(Bi, Sb)}$ antisites leads to Mn1, Mn2, and Mn3 sublattices (Figure 1a).[38] Since the Mn2 spins are always antiferromagnetically coupled with the Mn1, we will, for simplicity, focus on the Mn1 sublattice. In MBT, magnetism strongly couples with the charge carriers. Take $x = 0.48$, for example, upon cooling, $\rho(T)$ decreases with two slope changes (Figure 1b). One is at $T_N = 13.3$ K, associated with the PM to AFM transition of the Mn1 lattice. The other is a sharp resistivity drop at $T_{M1} = 9.7$ K, arising from the AFM to FM metamagnetic transition of the Mn1 spins. The sharp transition suggests the uniform doping of the sample, which is consistent with our WDS measurements.[38] With $H//c$, at 10 K, a sudden

https://doi.org/10.1021/acs.nanolett.2c01680
Nano Lett. 2022, 22, 5523−5529

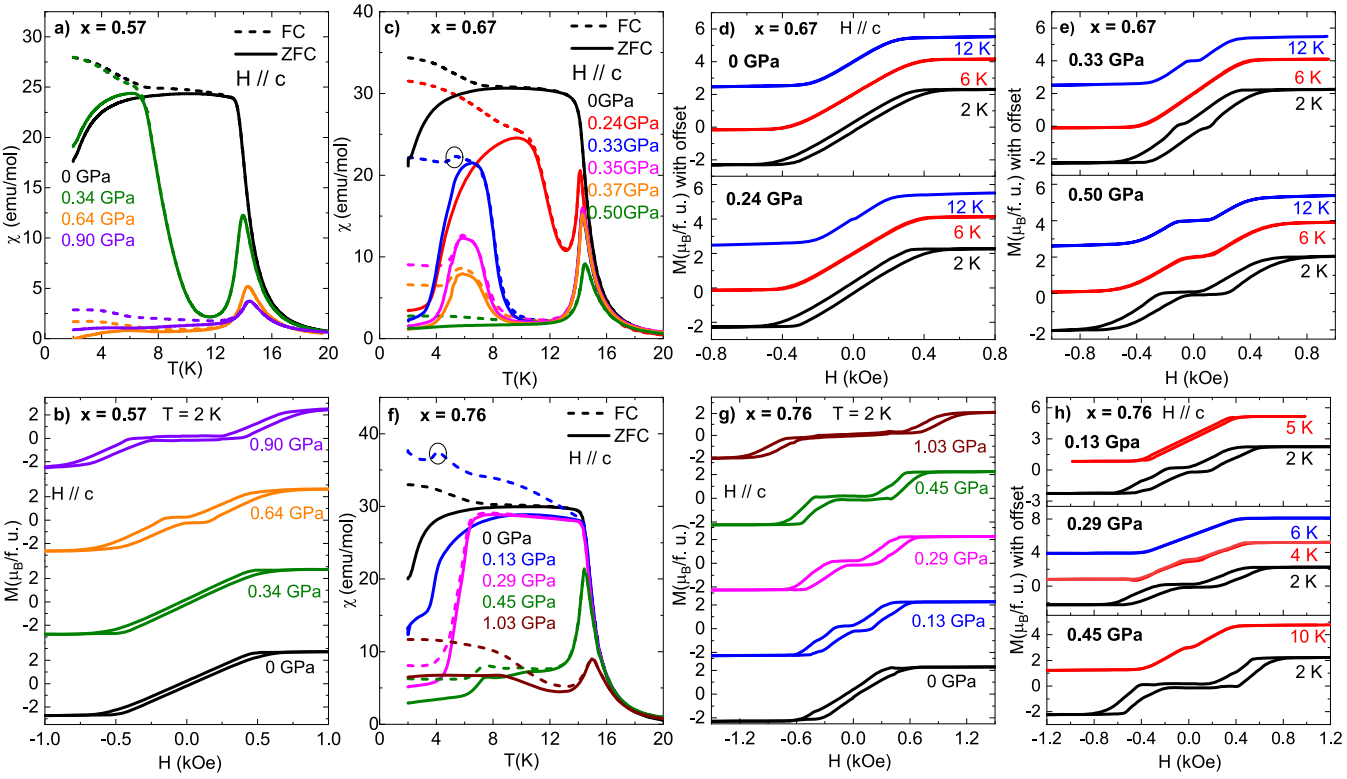

Figure 3. Effect of external pressures on the magnetic properties of $Mn(Bi_{1-x}Sb_x)_4Te_7$ (x = 0.57, 0.67 and 0.76): (a,c,f) Temperature dependent ZFC and FC magnetic susceptibility $\chi(T)$ with $H//c$. (b,g) Isothermal magnetization $M(H)$ at 2 K at different pressures for x = 0.57 (b) and 0.76 (g). (d,e,h) At fixed pressures, the $M(H)$ curves at different temperatures for x = 0.67 (d,e) and x = 0.76 (h). $M(H)$ data are analyzed to remove the lead signal, so slight discontinuity in data are induced.

decrease of MR appears at around 0.4 kOe by ∼5% due to the loss of spin disorder scattering from the AFM to the forced FM state.[38] In contrast, at 2 K, where the Mn1 spins are in the FM state, a weak monotonic decrease in MR occurs across the coercive field. In this Letter, together with the magnetic data, the distinct MR behaviors discussed above will be used to differentiate if the Mn1 spins are AFM or FM.

Five different doping levels were selected for the pressure study (Figure 2). For x = 0, at 0 GPa, $Mn(Bi_{1-x}Sb_x)_4Te_7$ is AFM below T_N = 12.2 K. T_N decreases slightly with pressure, similar to a previous study.[44] All MR curves at $P \leq 1.1$ GPa show a clear sudden drop, indicating that the system remains in the AFM state under pressure. For x = 0.48, T_N is essentially unaffected by pressure up to 1.97 GPa, the highest pressure we applied. In contrast, the FM to AFM metamagnetic transition at T_{M1} is extremely sensitive and becomes first-order like under pressure. At 0.89 GPa, T_{M1} is completely suppressed, leaving the ground state as AFM. Indeed, our MR data at 2 K (Figure 2g) shows a weak monotonic decrease for $P \leq 0.55$ GPa that is consistent with a FM ground state, while for $P \geq 0.89$ GPa, the sharp drop in MR reveals the AFM ground state. For x = 0.57, at 0 GPa, the PM to FM transition is revealed by the single resistivity anomaly at T_C and the weak monotonic MR decrease at 2 K. At 0.39 GPa, $\rho(T)$ shows two slope changes, suggesting the emergence of a pressure-induced AFM phase between T_N = 14.4 K and T_{M1} = 8.0 K. T_N slightly increases with pressure while T_{M1} is completely suppressed above 0.55 GPa. MR measurements confirm that the ground state is AFM for $P \leq 0.55$ GPa and FM for $P \geq 1.1$ GPa. For x = 0.67, although the pressure effect seems similar to that of x = 0.57, the ground state at 0.30 GPa is a puzzle. The $\rho(T)$ data implies PM → AFM → FM transitions and thus a FM ground state; however, the MR at 2 K shows a sharp drop, indicating an AFM ground state. These contradicting observations may suggest the re-entrance of AFM state, which will be discussed later. For x = 0.76, despite the envelope of $\rho(T)$ barely changing under pressure (Figure 2e), remarkably, the MR data suggests that this compound is the most sensitive to pressure among all, with the ground state being FM below 0.08 GPa and AFM above 0.25 GPa.

To further investigate the puzzling ground states, magnetic susceptibility $\chi(T)$ and isothermal magnetization $M(H)$ were measured with $H||c$ and shown in Figure 3. For x = 0.57, at ambient pressure, $\chi(T)$ shows a steep upturn plateau at T_C and a large bifurcation between the field-cooled (FC) and zero-field-cooled (ZFC) data; together with the typical hysteresis loop in $M(H)$ at 2 K, this indicates a FM ground state. At 0.34 GPa, the envelope of $\chi(T)$ evolves to show two anomalies. A cusp (PM to AFM) at T_N and a steep upturn plateau (AFM to FM) at T_{M1}. Under higher pressures, T_N slightly moves to higher temperature, while T_{M1} is completely suppressed above 0.64 GPa, where the $M(H)$ at 2 K shows the spin-flip feature, consistent with an AFM ground state. For x = 0.67, $\chi(T)$ resembles that of x = 0.57. However, closer examination of the 0.33 GPa data reveals that upon cooling, following the broad maximum, an additional "kink" feature highlighted by the circle in Figure 3c) emerges in the FC $\chi(T)$, suggesting three sequential magnetic transitions. Indeed, the $M(H)$ data shown in Figure 3d,e indicate complex phase transitions. In particular, at 0.33 GPa, it goes from PM to AFM at T_N, then the first metamagnetic transition from the AFM state to the FM state at T_{M1}, and then the second metamagnetic transition from the

https://doi.org/10.1021/acs.nanolett.2c01680
Nano Lett. 2022, 22, 5523−5529

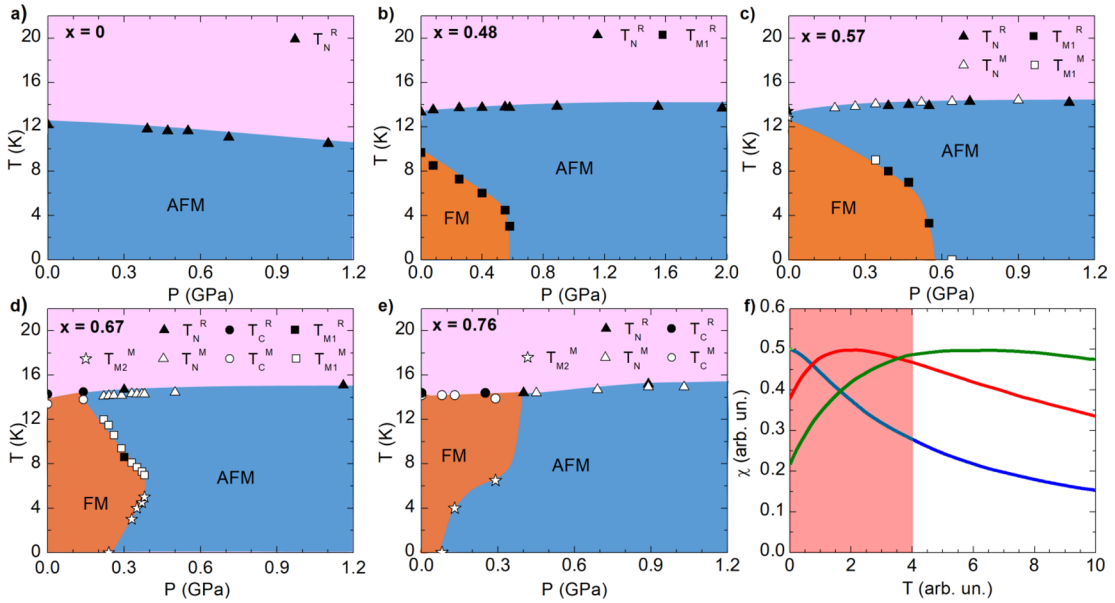

Figure 4. (a–e) Temperature–pressure (T–P) phase diagrams for $Mn(Bi_{1-x}Sb_x)_4Te_7$ (x = 0, 0.48, 0.57, 0.67, and 0.76) under pressures. T_C and T_N are the magnetic ordering temperatures of a PM to FM or AFM transition, respectively. T_{M1} and T_{M2} are the metamagnetic temperatures where an AFM → FM transition or a FM → AFM transition appears upon cooling, respectively. T_N^R, T_C^R, and T_{M1}^R were extracted by taking the first derivative of resistivity data. T_N^M, T_C^M, T_{M1}^M, and T_{M2}^M are determined by the first derivative of magnetic susceptibility data and then confirmed with isothermal magnetization measurements across critical temperatures. Note: the □/■ phase line representing the AFM to FM metamagnetic transition upon cooling is a first-order phase line, while the others are all second-order phase lines. (f) Typical behavior of susceptibility in a system with antiferromagnetic or spin-glass type correlations. The blue/red/green lines correspond to $T_{CW} \approx 3$, 7, and 15. Note that in a limited temperature range shown by pink shading, χ can either grow, decay, or show nonmonotonic behavior.

FM state to the AFM state at T_{M2}. For x = 0.76, at 0.13 GPa, following the broad maximum, a kink feature in FC $\chi(T)$ sets in at T_{M2} = 4.2 K which, together with Figure 3g, suggests a metamagnetic transition from a FM state to an AFM state at T_{M2}. T_{M2} increases under pressure, which manifests as a sharp drop in $\chi(T)$ at 0.29 GPa and then becomes a cusp feature at 0.45 GPa. The sequence of these phase transitions can also be inferred from the $M(H)$ data (Figure 3h). Upon cooling, at 0 GPa, it stays FM; at 0.13 and 0.29 GPa, it is FM → AFM; above 0.45 GPa, it remains AFM.

Figure 4a–e summarizes the temperature–pressure (T–P) phase diagrams. The upper phase line represents the ordering transition from the PM state to the ordered state, while the lower phase line marks the metamagnetic transitions between ordered states.

Several aspects are particularly unexpected, if not counterintuitive. First, as represented by the upper phase line, at sufficiently high doping levels (Figure 4d,e), the magnetic order switches suddenly from FM to AFM with pressure, yet the ordering temperature (T_C or T_N, respectively) is basically unchanged (a very tiny notch is barely discernible at the triple point at x = 0.76). Naïvely speaking, one would expect that at the triple point where the magnetic order is fully frustrated, the transition temperature, if at all existed, should be much lower. Second, pressure induces ferromagnetism at low temperature, but the order switches back to AFM upon cooling. Such FM to AFM metamagnetic transitions are rare (the best known example is FeRh)[45,46] and usually driven by the large volume effect at the metamagnetic transition (Clausius–Clapeyron theorem). This does not seem to be the case in our material, especially in view of the fact that the metamagnetic transitions marked with stars in Figure 4d,e are second-order and are unlikely to be due to the volume effect. Finally, the *sign* of the pressure coefficient of the metamagnetic transitions, dT_M/dP, varies with doping: $dT_M/dP < 0$ for $x \lesssim 0.6$, $dT_M/dP > 0$ for $x \gtrsim 0.7$, and for x = 0.67, it is positive at low and negative at higher temperatures.

These seemingly perplexing observations are all rooted in the unique separation of magnetic interaction in $Mn(Bi_{1-x}Sb_x)_4Te_7$. Indeed, it can be viewed, in a first approximation, as two overlapping magnetic subsystems, shaded in Figure 1a as pink and blue. In the discussion below, for simplicity, the former shall be referred to as Mn1 and the latter as Mn3.

Let us first consider Mn1. A single Mn1 layer forms a 2D magnetic system with strong FM intraplanar coupling $J > 0$ and weak interplanar coupling of varying sign $|J_\perp| \ll J$. In addition, it may have intraplanar magnetic anisotropy, which can, without loss of generality, be absorbed into a single-site term, so that the total magnetic Hamiltonian looks like

$$H_{11} = \sum_{ii'} J\mathbf{S_i}\cdot\mathbf{S_{i'}} + \sum_{ij} J_\perp \mathbf{S_i}\cdot\mathbf{S_j} + \sum_i K{S_{iz}}^2 \quad (1)$$

Here i, i' denote sites in the same layer, and i, j in the neighboring layers. For our system, $J < 0$ and $J_\perp > 0$.

Per the Mermin–Wagner theorem, in the 2D limit, a system does not order at any finite temperature if the exchange coupling is isotropic or if it has an easy-plane anisotropy ($K > 0$). On the other hand, a 2D easy-axis system with $K < 0$ and/or nonzero $J_\perp$ orders at a temperature generally determined as

$$T_c = \frac{a|J|}{b + \log(J/J_{\text{eff}})} \quad (2)$$

where a, b, and c are constants of the order of 1, and J_{eff} is a combination of $J_\perp$ and K that reduces to K in the $J_\perp \to 0$ limit.

https://doi.org/10.1021/acs.nanolett.2c01680
Nano Lett. 2022, 22, 5523–5529

For instance, in ref 47, an expression for J_{eff} was derived as $J_{\text{eff}} = K + J_\perp + \sqrt{K^2 + 2KJ_\perp}$.

According to the Stoner−Wohlfarth model,[48] for the $x = 0$ sample with the spin-flip transition, $|SJ_\perp| = g\mu_B H_c/z$ and $|SK| = g\mu_B(H_{ab} - 2H_c)/2$, where $H_{ab} = 1.2$ T is the field for the Mn1 spins to saturate along the ab plane and $H_c = 0.14$ T is the spin-flip field along the c axis, $g = 2$, $S = 5/2$, and $z = 2$ is the number of nearest Mn interlayer neighbors. The calculated $|SK| = 0.053$ meV and $|SJ_\perp| = 0.008$ meV. So, we conclude that our materials are in the regime where $K^2 \gg J_\perp^2$, where the ordering temperature (T_N or T_C) can be approximated as

$$T_c \approx \frac{a|J|}{b + \log(J/K)} \tag{3}$$

So T_c is only controlled by J and K, which characterize the intralayer magnetic dynamics. Specifically, T_c depends logarithmically weakly on the ratio of J/K. Thus, the ordering temperature is expected to be weakly pressure dependent, with maybe a tiny notch right at the triple point where $J_\perp$ is fully compensated. Indeed, in our experiment, T_N or T_C varies little in the entire set of experiments, between ∼11 K and ∼15 K.

Therefore, as a material system in the $K^2 \gg J_\perp^2$ regime, although the sign of $J_\perp$ defines the long-range order in the c direction, the ordering temperature depends logarithmically weakly on J/K. Consequently, neither T_N nor T_C is sensitive to the external pressures we applied (only up to 2 GPa) and is oblivious to the metamagnetic transitions under pressure.

Let us now turn to the pressure dependence of the metamagnetic transition. To understand it, we observe that a FM ordered Mn1 plane induces an exchange bias field H_{ex} in a magnetically disordered Mn3 layer. Assuming that the magnetic susceptibility of the latter is $\chi_3(T)$, we can add the fourth term to the Hamiltonian in eq 1, namely,

$$H_{13} = \pm\chi_3(T)H_{ex}^2 \tag{4}$$

where the plus sign corresponds to AFM stacking of the Mn1 plane and the minus to the FM stacking. Obviously, this Mn3-mediated interaction is always ferromagnetic and competes with the standard Mn1−Mn1 superexchange.[38]

Let us now estimate the pressure dependence of both interlayer terms using a simple Hubbard model. To this end, we consider two possible exchange paths. One is the "standard" superexchange, when an electron virtually hops from the effective Mn1 layer (which includes the entire pink region in Figure 1a) to anions in the effective Mn3 layer (Bi, Sb, or Te) and then to the next Mn1 layer. We will assign to Mn one effective d level, E_d, and to all anions one effective p level, E_p, with the charge transfer energy $\Delta E = E_d - E_p$ and a Hubbard repulsion U. The second exchange path is from the effective Mn1 to individual Mn3 ions. Importantly, E_p, E_d, and U are atomic parameters and are not sensitive to pressure. On the contrary, the hopping amplitudes, t_{pd} for the former path and t_{dd} for the latter are very sensitive to the interlayer distance.

The first path defines the standard AFM superexchange,

$$J_\perp^{\text{afm}} \propto t_{pd}^4/\Delta E^2 U \tag{5}$$

The second determines the exchange bias parameter in eq 4,

$$H_{ex} \propto t_{dd} \tag{6}$$

Per eq 4, this generates

$$J_\perp^{\text{fm}} \propto t_{dd}^2\chi_3(T) \tag{7}$$

Note that the same conclusion can be achieved by diagonalizing a three site Hubbard model with half-filling under an assumption that all sites have the same U and hopping $t_{12} = t_{13} = t_{dd}$.

Therefore, while both $J_\perp^{\text{afm}}$ and $J_\perp^{\text{fm}}$ are expected to increase with pressure, the former grows as the forth power of the effective hopping, and the latter only as the second power, making the AFM more favored under pressure. Since T_{M1} or T_{M2} is defined by $J_\perp$ (the transition occurs when it is fully compensated, $J_\perp = 0$), it is very sensitive to pressure because the AFM part grows much faster with pressure.

The most intriguing part is the exotic temperature dependence of the metamagnetic transition, with at least one concentration ($x = 0.67$) with the recurrent behavior. In order to understand that, recall that the only temperature-dependent parameter in eqs 5 and 7 is $\chi_3(T)$. Let us estimate its temperature dependence. For small doping levels we can neglect the internal interactions inside the Mn3 layer, so that $\chi_3(T)$ is described by the Curie law, $\chi_3(T) \propto 1/T$. At higher concentrations it is reasonable to assume (and this is also supported by neutron data) that the interactions in the Mn3 layer are random in sign and amplitude,[38] so on the mean field level they would freeze into a spin glass state with the net magnetization $\langle M_3 \rangle = 0$. While fluctuations beyond the mean field can completely destroy the spin-glass transition, or drive it to extremely low temperatures, the magnetic susceptibility of such systems would behave similar to that in a usual antiferromagnet. That is to say, the susceptibility will decay at high T as $\chi_3(T) \propto 1/(T + T_{CW})$ (we are using the convention where $T_{CW} > 0$ for the antiferromagnetic response) and has a maximum at some temperature $T_0 < T_{CW}$, and T_{CW} is on the order of the average interaction strength in the Mn3 plane. A typical $\chi_3(T)$ is shown in Figure 4f, where the approximate behavior of $\chi_3(T)$ for $T_{CW} = 3$, 7, and 15 is plotted (in arbitrary units). Note that T_{CW} is growing with the concentration, first very weakly, then rapidly. Therefore, the temperature range of interest (the shaded region in Figure 4) may fall either entirely in the range of $\chi_3(T)$ decreasing with temperature (small concentration of Mn3) or entirely in the range of increasing $\chi_3(T)$ (large concentrations) or even span both regimes (intermediate concentrations).

Now we summarize the microscopic explanation of all nontrivial behaviors we observed. For $x = 0$, the Mn3 concentration is very low, so $J_\perp^{\text{afm}} > J_\perp^{\text{fm}}$ holds below T_N for all pressures. For $x = 0.48$ and 0.57, the relatively larger Mn3 concentration (still low concentration case) makes $J_\perp^{\text{fm}}$ strong enough to compete with $J_\perp^{\text{afm}}$. Since χ_3 and thus $J_\perp^{\text{fm}}$ increase upon cooling, below the ordering temperature, an AFM to FM transition appears at T_{M1}. Upon compressing, $J_\perp^{\text{afm}}$ increases faster than $J_\perp^{\text{fm}}$, so T_{M1} decreases with pressure. For $x = 0.67$ (intermediate concentration case), at low pressures, $J_\perp^{\text{fm}} > J_\perp^{\text{afm}}$ holds for $T < T_C$. However, above a threshold pressure, $J_\perp^{\text{afm}}$ is favored over $J_\perp^{\text{fm}}$ at T_N. Then upon cooling, χ_3 and $J_\perp^{\text{fm}}$ first rise and then decrease, so an AFM to FM transition appears at T_{M1} and then a FM to AFM transition shows up at T_{M2}. Finally, with increasing pressure, the faster growing $J_\perp^{\text{afm}}$ leads to decreasing T_{M1} and increasing T_{M2}. For $x = 0.76$, χ_3 decreases upon cooling (large concentration case) as well as $J_\perp^{\text{fm}}$. Therefore, the FM to AFM transition occurs at $T_{M2} < T_C$. With increasing pressure, $J_\perp^{\text{afm}}$ grows faster, thus T_{M2} increases with pressure.

https://doi.org/10.1021/acs.nanolett.2c01680
Nano Lett. 2022, 22, 5523−5529

In summary, in $Mn(Bi_{1-x}Sb_x)_4Te_7$ where the antiferromagnetic superexchange interaction through anions and the Mn3-mediated ferromagnetic exchange interaction compete, we discover rare pressure-activated metamagnetic transitions with nontrivial pressure- and temperature-dependence and even reentrance. These unconventional behaviors are attributed to the distinct pressure and temperature dependence of the two competing interlayer exchange interactions. Moreover, we find the pressure effect on the ordering temperature from the PM to ordered state is weak, which we further show to be due to its logarithmically weakly dependence on the ratio of the intralayer coupling and magnetic anisotropy. Therefore, our study provides independent probing of the interlayer coupling, intralayer coupling, and magnetic anisotropy and the role that they play in van der Waals magnetism.

■ ASSOCIATED CONTENT

Supporting Information

The Supporting Information is available free of charge at https://pubs.acs.org/doi/10.1021/acs.nanolett.2c01680.

Single crystal growth and characterization, magnetic and electrical property measurements at ambient pressure, and measurement details under pressure (PDF)

■ AUTHOR INFORMATION

Corresponding Author

Ni Ni − *Department of Physics and Astronomy and California NanoSystems Institute, University of California, Los Angeles, Los Angeles, California 90095, United States*; Email: nini@physics.ucla.edu

Authors

Tiema Qian − *Department of Physics and Astronomy and California NanoSystems Institute, University of California, Los Angeles, Los Angeles, California 90095, United States*; orcid.org/0000-0003-4673-5662

Eve Emmanouilidou − *Department of Physics and Astronomy and California NanoSystems Institute, University of California, Los Angeles, Los Angeles, California 90095, United States*

Chaowei Hu − *Department of Physics and Astronomy and California NanoSystems Institute, University of California, Los Angeles, Los Angeles, California 90095, United States*

Jazmine C. Green − *Department of Physics and Astronomy and California NanoSystems Institute, University of California, Los Angeles, Los Angeles, California 90095, United States*

Igor I. Mazin − *Department of Physics and Astronomy, George Mason University, Fairfax, Virginia 22030, United States; Quantum Science and Engineering Center, George Mason University, Fairfax, Virginia 22030, United States*; orcid.org/0000-0001-9456-7099

Complete contact information is available at: https://pubs.acs.org/10.1021/acs.nanolett.2c01680

Author Contributions

§T.Q. and E.E. contributed equally to this work.

Notes

The authors declare no competing financial interest.

■ ACKNOWLEDGMENTS

Work at UCLA was supported by the U.S. Department of Energy (DOE), Office of Science, Office of Basic Energy Sciences under Award Number DE-SC0021117. I.I.M. acknowledges support from DOE under the Grant DE-SC0021089. C.H. acknowledges the support by the Julian Schwinger Fellowship at UCLA.

■ REFERENCES

(1) Novoselov, K. S.; Mishchenko, A.; Carvalho, A.; Castro Neto, A. H. 2D materials and van der Waals heterostructures. *Science* **2016**, *353*, aac9439.

(2) Gong, C.; Li, L.; Li, Z.; Ji, H.; Stern, A.; Xia, Y.; Cao, T.; Bao, W.; Wang, C.; Wang, Y.; et al. Discovery of intrinsic ferromagnetism in two-dimensional van der Waals crystals. *Nature* **2017**, *546*, 265−269.

(3) Deng, Y.; Yu, Y.; Song, Y.; Zhang, J.; Wang, N. Z.; Sun, Z.; Yi, Y.; Wu, Y. Z.; Wu, S.; Zhu, J.; et al. Gate-tunable room-temperature ferromagnetism in two-dimensional Fe_3GeTe_2. *Nature* **2018**, *563*, 94−99.

(4) Wang, Z.; Zhang, T.; Ding, M.; Dong, B.; Li, Y.; Chen, M.; Li, X.; Huang, J.; Wang, H.; Zhao, X.; et al. Electric-field control of magnetism in a few-layered van der Waals ferromagnetic semiconductor. *Nature Nanotechnol.* **2018**, *13*, 554−559.

(5) Sun, X.; Li, W.; Wang, X.; Sui, Q.; Zhang, T.; Wang, Z.; Liu, L.; Li, D.; Feng, S.; Zhong, S.; et al. Room temperature ferromagnetism in ultra-thin van der Waals crystals of 1T-$CrTe_2$. *Nano Research* **2020**, *13*, 3358−3363.

(6) May, A. F.; Ovchinnikov, D.; Zheng, Q.; Hermann, R.; Calder, S.; Huang, B.; Fei, Z.; Liu, Y.; Xu, X.; McGuire, M. A. Ferromagnetism near room temperature in the cleavable van der Waals crystal Fe_3GeTe_2. *ACS Nano* **2019**, *13*, 4436−4442.

(7) Gati, E.; Inagaki, Y.; Kong, T.; Cava, R. J.; Furukawa, Y.; Canfield, P. C.; Bud'Ko, S. L. Multiple ferromagnetic transitions and structural distortion in the van der Waals ferromagnet VI_3 at ambient and finite pressures. *Phys. Rev. B* **2019**, *100*, 094408.

(8) Huang, B.; Clark, G.; Navarro-Moratalla, E.; Klein, D. R.; Cheng, R.; Seyler, K. L.; Zhong, D.; Schmidgall, E.; McGuire, M. A.; Cobden, D. H.; et al. Layer-dependent ferromagnetism in a van der Waals crystal down to the monolayer limit. *Nature* **2017**, *546*, 270−273.

(9) Huang, B.; Clark, G.; Klein, D. R.; MacNeill, D.; Navarro-Moratalla, E.; Seyler, K. L.; Wilson, N.; McGuire, M. A.; Cobden, D. H.; Xiao, D.; et al. Electrical control of 2D magnetism in bilayer CrI_3. *Nature Nanotechnol.* **2018**, *13*, 544−548.

(10) Jiang, S.; Li, L.; Wang, Z.; Mak, K. F.; Shan, J. Controlling magnetism in 2D CrI_3 by electrostatic doping. *Nature Nanotechnol.* **2018**, *13*, 549−553.

(11) Jiang, S.; Shan, J.; Mak, K. F. Electric-field switching of two-dimensional van der Waals magnets. *Nature materials* **2018**, *17*, 406−410.

(12) Webster, L.; Yan, J.-A. Strain-tunable magnetic anisotropy in monolayer $CrCl_3$, $CrBr_3$, and CrI_3. *Phys. Rev. B* **2018**, *98*, 144411.

(13) Wu, Z.; Yu, J.; Yuan, S. Strain-tunable magnetic and electronic properties of monolayer CrI_3. *Phys. Chem. Chem. Phys.* **2019**, *21*, 7750−7755.

(14) Song, T.; Fei, Z.; Yankowitz, M.; Lin, Z.; Jiang, Q.; Hwangbo, K.; Zhang, Q.; Sun, B.; Taniguchi, T.; Watanabe, K.; et al. Switching 2D magnetic states via pressure tuning of layer stacking. *Nature materials* **2019**, *18*, 1298−1302.

(15) Cenker, J.; Sivakumar, S.; Xie, K.; Miller, A.; Thijssen, P.; Liu, Z.; Dismukes, A.; Fonseca, J.; Anderson, E.; Zhu, X.; Roy, X.; Xiao, D.; Chu, J.-H.; Cao, T.; Xu, X. Reversible strain-induced magnetic phase transition in a van der Waals magnet. *Nat. Nanotechnol.* **2022**, *17* (3), 256−261.

(16) Wilson, N. P.; Lee, K.; Cenker, J.; Xie, K.; Dismukes, A. H.; Telford, E. J.; Fonseca, J.; Sivakumar, S.; Dean, C.; Cao, T.; et al. Interlayer electronic coupling on demand in a 2D magnetic semiconductor. *Nat. Mater.* **2021**, *20*, 1657−1662.

(17) Lee, D. S.; Kim, T.-H.; Park, C.-H.; Chung, C.-Y.; Lim, Y. S.; Seo, W.-S.; Park, H.-H. Crystal structure, properties and nanostructuring of a new layered chalcogenide semiconductor, Bi_2MnTe_4. *CrystEngComm* **2013**, *15*, 5532−5538.
(18) Otrokov, M. M.; Klimovskikh, I. I.; Bentmann, H.; Estyunin, D.; Zeugner, A.; Aliev, Z. S.; Gaß, S.; Wolter, A.; Koroleva, A.; Shikin, A. M.; et al. Prediction and observation of an antiferromagnetic topological insulator. *Nature* **2019**, *576*, 416−422.
(19) Zhang, D.; Shi, M.; Zhu, T.; Xing, D.; Zhang, H.; Wang, J. Topological axion states in the magnetic insulator $MnBi_2Te_4$ with the quantized magnetoelectric effect. *Physical review letters* **2019**, *122*, 206401.
(20) Li, J.; Li, Y.; Du, S.; Wang, Z.; Gu, B.-L.; Zhang, S.-C.; He, K.; Duan, W.; Xu, Y. Intrinsic magnetic topological insulators in van der Waals layered $MnBi_2Te_4$-family materials. *Science Advances* **2019**, *5*, No. eaaw5685.
(21) Aliev, Z. S.; Amiraslanov, I. R.; Nasonova, D. I.; Shevelkov, A. V.; Abdullayev, N. A.; Jahangirli, Z. A.; Orujlu, E. N.; Otrokov, M. M.; Mamedov, N. T.; Babanly, M. B.; et al. Novel ternary layered manganese bismuth tellurides of the MnTe-Bi_2Te_3 system: Synthesis and crystal structure. *J. Alloys Compd.* **2019**, *789*, 443−450.
(22) Otrokov, M. M.; Rusinov, I. P.; Blanco-Rey, M.; Hoffmann, M.; Vyazovskaya, A. Y.; Eremeev, S. V.; Ernst, A.; Echenique, P. M.; Arnau, A.; Chulkov, E. V. Unique thickness-dependent properties of the van der Waals interlayer antiferromagnet $MnBi_2Te_4$ films. *Phys. Rev. Lett.* **2019**, *122*, 107202.
(23) Hu, S.; Yi, J.; Zhang, Y.-J.; Lin, K.-Q.; Liu, B.-J.; Chen, L.; Zhan, C.; Lei, Z.-C.; Sun, J.-J.; Zong, C.; Li, J.-F.; Ren, B. A van der Waals antiferromagnetic topological insulator with weak interlayer magnetic coupling. *Nat. Commun.* **2020**, *11*, 2518.
(24) Wu, J.; Liu, F.; Sasase, M.; Ienaga, K.; Obata, Y.; Yukawa, R.; Horiba, K.; Kumigashira, H.; Okuma, S.; Inoshita, T.; Hosono, H.; et al. Natural van der Waals heterostructural single crystals with both magnetic and topological properties. *Science Advances* **2019**, *5*, No. eaax9989.
(25) Hu, C.; Ding, L.; Gordon, K. N.; Ghosh, B.; Tien, H.-J.; Li, H.; Linn, A. G.; Lien, S.-W.; Huang, C.-Y.; Mackey, S.; et al. Realization of an intrinsic ferromagnetic topological state in $MnBi_8Te_{13}$. *Science Advances* **2020**, *6*, No. eaba4275.
(26) Klimovskikh, I. I.; Otrokov, M. M.; Estyunin, D.; Eremeev, S. V.; Filnov, S. O.; Koroleva, A.; Shevchenko, E.; Voroshnin, V.; Rybkin, A. G.; Rusinov, I. P.; et al. Tunable 3D/2D magnetism in the $(MnBi_2Te_4)(Bi_2Te_3)_m$ topological insulators family. *npj Quantum Materials* **2020**, *5*, 54.
(27) Shi, M.; Lei, B.; Zhu, C.; Ma, D.; Cui, J.; Sun, Z.; Ying, J.; Chen, X. Magnetic and transport properties in the magnetic topological insulators $MnBi_2Te_4$ $(Bi_2Te_3)_n$ (n= 1, 2). *Phys. Rev. B* **2019**, *100*, 155144.
(28) Lee, S. H.; Zhu, Y.; Wang, Y.; Miao, L.; Pillsbury, T.; Yi, H.; Kempinger, S.; Hu, J.; Heikes, C. A.; Quarterman, P.; et al. Spin scattering and noncollinear spin structure-induced intrinsic anomalous Hall effect in antiferromagnetic topological insulator $MnBi_2Te_4$. *Physical Review Research* **2019**, *1*, 012011.
(29) Tian, S.; Gao, S.; Nie, S.; Qian, Y.; Gong, C.; Fu, Y.; Li, H.; Fan, W.; Zhang, P.; Kondo, T.; et al. Magnetic topological insulator $MnBi_6Te_{10}$ with a zero-field ferromagnetic state and gapped Dirac surface states. *Phys. Rev. B* **2020**, *102*, 035144.
(30) Gordon, K. N.; Sun, H.; Hu, C.; Linn, A. G.; Li, H.; Liu, Y.; Liu, P.; Mackey, S.; Liu, Q.; Ni, N. Strongly Gapped Topological Surface States on Protected Surfaces of Antiferromagnetic $MnBi_4Te_7$ and $MnBi_6Te_{10}$. *arXiv* **2019**, 1910.13943.
(31) Deng, Y.; Yu, Y.; Shi, M. Z.; Guo, Z.; Xu, Z.; Wang, J.; Chen, X. H.; Zhang, Y. Quantum anomalous Hall effect in intrinsic magnetic topological insulator $MnBi_2Te_4$. *Science* **2020**, *367*, 895−900.
(32) Liu, C.; Wang, Y.; Li, H.; Wu, Y.; Li, Y.; Li, J.; He, K.; Xu, Y.; Zhang, J.; Wang, Y. Robust axion insulator and Chern insulator phases in a two-dimensional antiferromagnetic topological insulator. *Nat. Mater.* **2020**, *19*, 522−527.
(33) Ge, J.; Liu, Y.; Li, J.; Li, H.; Luo, T.; Wu, Y.; Xu, Y.; Wang, J. High-Chern-number and high-temperature quantum Hall effect without Landau levels. *National science review* **2020**, *7*, 1280−1287.
(34) Gao, A.; Liu, Y.-F.; Hu, C.; Qiu, J.-X.; Tzschaschel, C.; Ghosh, B.; Ho, S.-C.; Bérubé, D.; Chen, R.; Sun, H.; et al. Layer Hall effect in a 2D topological axion antiferromagnet. *Nature* **2021**, *595*, 521−525.
(35) Yan, C.; Zhu, Y.; Fernandez-Mulligan, S.; Green, E.; Mei, R.; Yan, B.; Liu, C.; Mao, Z.; Yang, S. Delicate Ferromagnetism in $MnBi_6Te_{10}$. *arXiv* **2021**, 2107.08137.
(36) Chen, W.; Hu, Y.; Lv, W.; Lei, T.; Wang, X.; Li, Z.; Zhang, M.; Huang, J.; Du, X.; Yan, Y.; He, W.; Liu, C.; Liao, M.; Zhang, W.; Xiong, J.; Yan, C. Intrinsic magnetic topological insulator phases in the Sb doped $MnBi_2Te_4$ bulks and thin flakes. *Nat. Commun.* **2019**, *10*, 4973.
(37) Yan, J.-Q.; Okamoto, S.; McGuire, M. A.; May, A. F.; McQueeney, R. J.; Sales, B. C. Evolution of structural, magnetic, and transport properties in $MnBi_{2-x}Sb_xTe_4$. *Phys. Rev. B* **2019**, *100*, 104409.
(38) Hu, C.; Lien, S.-W.; Feng, E.; Mackey, S.; Tien, H.-J.; Mazin, I. I.; Cao, H.; Chang, T.-R.; Ni, N. Tuning magnetism and band topology through antisite defects in Sb-doped $MnBi_4Te_7$. *Phys. Rev. B* **2021**, *104*, 054422.
(39) Liu, Y.; Wang, L.-L.; Zheng, Q.; Huang, Z.; Wang, X.; Chi, M.; Wu, Y.; Chakoumakos, B. C.; McGuire, M. A.; Sales, B. C.; et al. Site Mixing for Engineering Magnetic Topological Insulators. *Physical Review X* **2021**, *11*, 021033.
(40) Xie, H.; Fei, F.; Fang, F.; Chen, B.; Guo, J.; Du, Y.; Qi, W.; Pei, Y.; Wang, T.; Naveed, M.; et al. Charge carrier mediation and ferromagnetism induced in $MnBi_6Te_{10}$ magnetic topological insulators by antimony doping. *J. Phys. D: Appl. Phys.* **2022**, *55*, 104002.
(41) Chen, K.; Wang, B.; Yan, J.-Q.; Parker, D.; Zhou, J.-S.; Uwatoko, Y.; Cheng, J.-G. Suppression of the antiferromagnetic metallic state in the pressurized $MnBi_2Te_4$ single crystal. *Physical Review Materials* **2019**, *3*, 094201.
(42) Pei, C.; Xia, Y.; Wu, J.; Zhao, Y.; Gao, L.; Ying, T.; Gao, B.; Li, N.; Yang, W.; Zhang, D.; et al. Pressure-induced topological and structural phase transitions in an antiferromagnetic topological insulator. *Chin. Phys. Lett.* **2020**, *37*, 066401.
(43) Pei, C.; Xi, M.; Wang, Q.; Shi, W.; Gao, L.; Zhao, Y.; Tian, S.; Cao, W.; Li, C.; Zhang, M. Pressure-Induced Superconductivity and Structural Phase Transitions in Magnetic Topological Insulator Candidate $MnSb_4Te_7$. *arXiv* **2022**, 2201.07635.
(44) Shao, J.; Liu, Y.; Zeng, M.; Li, J.; Wu, X.; Ma, X.-M.; Jin, F.; Lu, R.; Sun, Y.; Gu, M.; et al. Pressure-tuned intralayer exchange in superlattice-like $MnBi_2Te_4/(Bi_2Te_3)$ n topological insulators. *Nano Lett.* **2021**, *21*, 5874−5880.
(45) Vinokurova, L.; Vlasov, A.; Pardavi-Horváth, M. Pressure effects on magnetic phase transitions in FeRh and FeRhIr alloys. *physica status solidi (b)* **1976**, *78*, 353−357.
(46) Stern-Taulats, E.; Castán, T.; Planes, A.; Lewis, L. H.; Barua, R.; Pramanick, S.; Majumdar, S.; Manosa, L. Giant multicaloric response of bulk Fe 49 Rh 51. *Phys. Rev. B* **2017**, *95*, 104424.
(47) Katanin, A. A.; Katanin, A. A.; Irkhin, V. Y. Magnetic order and spin fluctuations in low-dimensional insulating systems. *Physics-Uspekhi* **2007**, *50*, 613.
(48) Stoner, E. C.; Wohlfarth, E. A mechanism of magnetic hysteresis in heterogeneous alloys. *Philosophical Transactions of the Royal Society of London. Series A, Mathematical and Physical Sciences* **1948**, *240*, 599.

NOTE ADDED AFTER ASAP PUBLICATION

This paper was published ASAP on June 22, 2022, with the last name of the second author misspelled. The corrected version was reposted on June 23, 2022.

https://doi.org/10.1021/acs.nanolett.2c01680
Nano Lett. 2022, 22, 5523−5529

supporting information for "Unconventional pressure-driven metamagnetic transitions in topological van der Waals magnets"

Tiema Qian,[†] Eve Emmanouilidou,[†] Chaowei Hu,[†] Jazmine C. Green,[†] Igor I. Mazin,[‡,¶] and Ni Ni[*,†]

[†]*Department of Physics and Astronomy and California NanoSystems Institute, University of California, Los Angeles, Los Angeles, CA 90095, USA*

[‡]*Department of Physics and Astronomy, George Mason University, Fairfax, VA 22030, USA*

[¶]*Quantum Science and Engineering Center, George Mason University, Fairfax, VA 22030, USA*

E-mail: nini@physics.ucla.edu

Single crystal growth and characterization.

Single crystals were grown using the flux method.[1] Powder X-ray diffraction was performed via a PANalytical Empyrean diffractometer (Cu Kα radiation) to determine the phase purity. The Sb doping levels of the $Mn(Bi_{1-x}Sb_x)_4Te_7$ crystals refer to the actual concentrations, determined by wavelength dispersive spectroscopy.

Magnetic and electrical property measurements.

Magnetic susceptibility and isothermal magnetization measurements under pressure were performed in a Quantum Design (QD) Magnetic Property Measurement System (MPMS3) with $H//c$. Electrical transport measurements were performed in a QD DynaCool Physical Property Measurement System (PPMS). Resistivity and magnetoresistance measurements were performed using the four-probe method, with $I//ab$ and $H//c$. To eliminate unwanted contributions from mixed transport channels of the magnetotransport data, data were collected while sweeping the magnetic field from -9 T to 9 T. The data were then symmetrized to obtain $\rho_{xx}(H)$ using $\rho_{xx}(H) = (\rho_{xx}(H) + \rho_{xx}(-H))/2$. The MR was defined as $(\rho_{xx}(H) - \rho_{xx}(0))/\rho_{xx}(0)$.

Measurements under pressures.

For the transport properties under pressure, a C&T Factory commercial piston pressure cell compatible with a QD PPMS was used; for the magnetic properties under pressure, a HMD pressure cell compatible with a QD MPMS3 was applied. Daphne Oil 7373[2] was used as the hydrostatic pressure medium. A Pb piece was used as a manometer by tracking the pressure dependence of its superconducting transition, which is described by $dT_c/dP = -0.361(5)$ K/GPa.[3] The magnetic signal from Pb was subtracted from the total magnetic signal to obtain the magnetic data of the samples.

References

(1) Hu, C.; Lien, S.-W.; Feng, E.; Mackey, S.; Tien, H.-J.; Mazin, I. I.; Cao, H.; Chang, T.-R.; Ni, N. Tuning magnetism and band topology through antisite defects in Sb-doped $MnBi_4Te_7$. *Physical Review B* **2021**, *104*, 054422.

(2) Yokogawa, K.; Murata, K.; Yoshino, H.; Aoyama, S. Solidification of high-pressure medium Daphne 7373. *Japanese journal of applied physics* **2007**, *46*, 3636.

(3) Clark, M.; Smith, T. Pressure dependence of T_c for lead. *Journal of Low Temperature Physics* **1978**, *32*, 495–503.